atmosphere

MDPI

Article

Quantification of Urban Methane Emissions: A Combination of Stationary with Mobile Measurements

Florian Kurt Kohler, Carsten Schaller and Otto Klemm *

Climatology Research Group, University of Münster, 48149 Münster, Germany
* Correspondence: otto.klemm@uni-muenster.de

Abstract: The mixing ratios of methane (CH_4) were recorded with high temporal and spatial resolution in Münster, Germany, to identify urban CH_4 sources and to quantify the overall inner city CH_4 emissions. Both mobile and stationary measurement techniques were employed. The background mixing ratios showed a diurnal cycle with higher values at night under stable stratification conditions. In the industrial park, periodic peaks were detected. Ten mappings of the urban CH_4 mixing ratio were made with an instrumented cargo bicycle. Repeated local increases in mixing ratios were found at 13 individual locations. The emission rate was estimated to be 22.0 g h^{-1} km^{-1}. A total of five leaks from the underground gas distribution network were identified. From the increase in background mixing ratio, the overall source strength of the study area was estimated to be 24.6 g m^{-2} a^{-1}, which is approximately three times the total CH_4 emissions from the city's most recent emissions report. The contribution of point sources was 0.64 g m^{-2} a^{-1}, suggesting that significant additional CH_4 sources exist within the study area. In the interest of climate protection, there is an urgent need for further research on the urban CH_4 sources and emission fluxes in detail.

Keywords: urban CH_4 emissions; point sources; urban diurnal CH_4 cycle; mobile and stationary measurements

check for updates

Citation: Kohler, F.K.; Schaller, C.; Klemm, O. Quantification of Urban Methane Emissions: A Combination of Stationary with Mobile Measurements. *Atmosphere* **2022**, *13*, 1596. https://doi.org/10.3390/atmos13101596

Academic Editors: David Reed and Ari Preston

Received: 28 August 2022
Accepted: 27 September 2022
Published: 29 September 2022

1. Introduction

Methane (CH_4) is an important trace gas in the atmosphere, and, in terms of climate forcing, it is the second most important anthropogenic greenhouse gas after carbon dioxide (CO_2) [1]. Compared to CO_2, CH_4 has a stronger warming potential and has seen increases in atmospheric concentration in recent decades despite having a shorter atmospheric residence time [2]. Global atmospheric CH_4 concentrations have been increasing since the beginning of the industrial era, largely due to anthropogenic emissions from agriculture (e.g., animal husbandry, rice cultivation, biomass burning), fossil fuel production and use, and waste disposal. The anthropogenic share of annual global CH_4 emissions is estimated to be about 60% [2]. Today's atmospheric CH_4 mixing ratio of 1.877 ppm (in 2019) is about 2.6 times the estimated preindustrial level in 1750 [3].

With an atmospheric residence time of about nine years, CH_4 is one of the more short-lived greenhouse gases [4]. Therefore, reducing CH_4 emissions results in the rapid stabilization or reduction in its atmospheric concentration and, thus, its radiative forcing [5]. Therefore, reducing CH_4 emissions is an effective option for rapid action against global warming [6,7], consistent with achieving the goals of the Paris Agreement.

Reducing atmospheric CH_4 concentrations begins with finding, identifying, and quantifying CH_4 emissions [6]. Urban areas form a complex environment where multiple potential sources of CH_4 coexist; these sources include heating systems (oil and gas grids and combustion systems), landfills, wastewater systems, and road traffic [8–10].

Various studies have aimed to quantify CH_4 emissions in urban areas. Helfter et al. [11] detected CH_4 fluxes from urban areas in London, UK, with moderate seasonality (though greater emissions in winter). The determined annual CH_4 emissions were twice as high as

indicated in the City of London's annual emissions report. Other studies also show that estimates of CH_4 emissions from "top-down" approaches (atmospheric measurements) are often larger than CH_4 emissions estimated by "bottom-up" approaches (evaluation of statistical data and emission factors) [12–16]. Closing this discrepancy will require improved measurement techniques and a well-distributed network of measurement stations [17]. To date, researchers still lack a basic understanding of the locations and temporal patterns of urban CH_4 sources [8,18,19].

Highly sensitive mobile measurement systems have been shown to be an effective method for detecting CH_4 concentrations in a short time over large spatial areas and identifying point sources and gas leaks [8,19–23]. Weller et al. [21] were able to detect point sources with a frequency of 0.19 to 0.30 km^{-1} along urban streets by using mobile measurement platforms in four different cities in the U.S. In the European cities of Utrecht (Netherlands) and Hamburg (Germany), Maazallahi et al. [19] identified point sources, of which one of three in Hamburg and two of three in Utrecht had fossil origin. In Hamburg, 20% of the point sources of fossil origin could be identified as gas leaks, which were responsible for a total of 50% of the estimated emissions from the identified point sources.

Münster is a city with just over 300,000 inhabitants, located in flat terrain in NW Germany. It hosts light industry as well as small- and medium-sized industry and is surrounded by heavy agriculture. Two main traffic routes pass by Münster in an S–N direction, the federal motorway #1 and the major waterway Dortmund–Ems Canal for cargo ships. Today, Münster's former commercial harbor is used for small-scale leisure activities. Since 2005, the municipal utilities have operated a combined cycle power plant (CCPP) and a combined heat and power plant (CHP) within the industrial park at the city harbor. The more efficient CCPP replaced the previously coal-fired power plant and has since contributed to savings in annual CO_2 emissions (improving the emission factor for the local electricity mix from 750 g kWh^{-1} in 2000 to 474 g kWh^{-1} in 2019 [24]). Based on the principle of co-generation, natural gas is burned in the CCPP and converted into electrical energy (output: 100 MW) and thermal energy (output: 200 MW). The CCPP thus covers up to 50% of Münster's electricity requirements and up to 20% of its heat requirements [25]. According to the same principle, biomethane is burned and converted into electrical (output: 3.9 MW), thermal (output: 4.1 MW), and combustion heat energy (output: 9.3 MW) in the CHP [26]. The CHP serves as a backup power generator but also supports the CCPP during regular operation [27]. In addition, another 12 CHP are operated in the city of Münster [28]. The city has a well-developed gas pipeline network with a total length of 975 km. Gas is fed in at eight points and fed out at a total of 38,264 connections for small businesses and household heating and cooking facilities [29].

In 2017, the bottom-up estimate of Münster's CH_4 emissions was 80,000 t CO_2-equivalents [30]. However, Münster, similar to other cities in NW Germany, does not systematically record CH_4 concentrations [31,32], so a top-down estimate of CH_4 emissions cannot be made. Since a study of the CO_2 emissions in Münster yielded a top-down estimate that was 3.3 times smaller than the bottom-up estimate [33], this study aims to determine whether such a discrepancy exists for CH_4 emissions in Münster, specifically by estimating CH_4 emissions using a top-down approach. We used a novel combination of stationary and mobile measurement techniques to determine the overall source strength of the urban environment as well as to identify point sources and emission rates.

2. Experimental Design

2.1. Stationary Measurements

From 12 December 2020 to 7 March 2021, two stationary CH_4 measuring stations were operated in the urban area of Münster, Germany (Figure 1). Measuring station MS4.9 was located in the industrial area at the city harbor at a height of 4.9 m above ground level (agl) and 20 m northeast of a power plant (combined cycle gas turbine plant (CCGT) and combined heat and power plant (CHP)) operated by the municipal utility operations. A tower for the installation of the sensors was erected on an overseas container (51.950529 N,

7.642013 E), close to the street Am Mittelhafen. The mixing ratio of CH_4 was measured with an LI-7700 Open Path CH_4 Gas Analyzer (LI-COR Biosciences Inc., Lincoln, NE, USA) at a frequency of 1 Hz. The horizontal wind direction and speed were measured at a height of 5.4 m agl using the anemometer model WindSonic 2D (Gill Instruments Ltd., Lymington, Hampshire, UK). The data were recorded with a data logger (CR3000, Campbell Scientific Ltd., Shepshed, Leicestershire, UK).

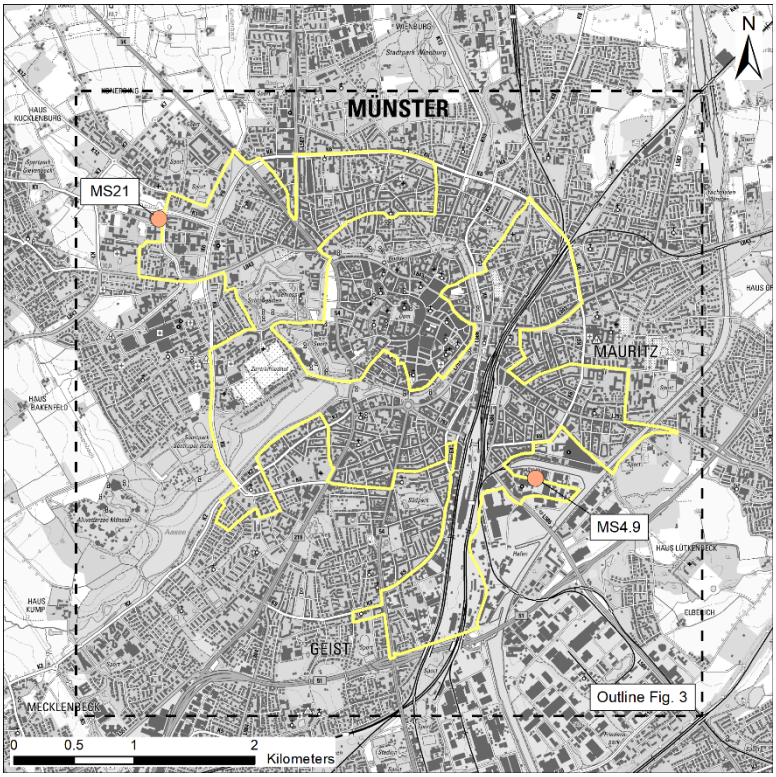

(**a**)

(**b**)

Figure 1. (**a**) City route for mobile measurements (MM) and location of stationary measuring stations MS21 and MS4.9: Map source: DTK25, 1:25,000, © Geobasis NRW 2017, DL-DE->Zero-2.0, (http://www.govdata.de/dl-de/zero-2-0, accessed on 1 November 2021). URL: https://www.bezreg-koeln.nrw.de/brk_internet/geobasis/topographische_karten/aktuell/25000/index.html (accessed on 1 November 2021); (**b**) Mobile station setup MM with CH_4 sensor (1), GPS receiver (2), display (3) and logger box including battery (4).

Measuring station MS21 was located 3.8 km from MS4.9 on the roof of the GEO 1 building of the University of Münster at Heisenbergstraße 2 (51.96942 N, 7.59588 E) in the western part of the city at a height of 21 m agl. The CH_4 mixing ratio was measured with the $CH_4/N_2O/H_2O$ Closed Path Analyzer LGR 913-1054 (Los Gatos Research Inc., San Jose, CA, USA) at a frequency of 1 Hz. The wind direction and velocity data (WindSonic 2D by Gill Instruments Ltd., Lymington, Hampshire, UK) were obtained from the weather station at the same site at a height of 34 m agl. Those averaged 10-min data serve as the undisturbed wind field. Furthermore, data on the air temperature (HC2S3, Campbell Scientific Ltd., Shepshed, Leicestershire, UK) and air pressure (61302V, R.M. Young Company, Traverse City, MI, USA) from the station were used. For both LI-7700 and LGR 913-1054, user calibration was applied according to the manufacturer's specifications with span calibration (2.04 ppm) and zero calibration. Schaller et al. [34] and Detto et al. [35] proved excellent agreement between the two devices.

Data on the stratification stability of the boundary layer during the whole observation period were taken from a measuring station located 1.2 km north of MS21 (51.980123 N,

7.599255 E) on a meadow 300 m outside the urban development. The air temperature (HC2S3 from Campbell Scientific Ltd., Shepshed, Leicestershire, UK) was measured at heights of 2 m and 10 m agl, averaged over 10 min. The stability classes, according to Klug [36]/Manier [37] and Pasquill [38], were calculated by using the vertical temperature gradient. Statements about the height of the boundary layer were made using data from the radiosonde of the German Weather Service (DWD) at the station Essen 10410 EDZE [39].

2.2. Mobile Measurements

At 10 points in time during the period January to March 2021, mobile measurement data were collected with a converted cargo bicycle. The mobile measurement station MM was equipped with an LI-7700 Open Path CH_4 Gas Analyzer (LI-COR Biosciences Inc., Lincoln, NE, USA) mounted horizontally at a height of 0.68 m agl to measure the CH_4 mixing ratio, and it had a GPS receiver (19 × HVS, Garmin International Inc., Olathe, KS, USA) for positioning (Figure 1). The measured data (10 Hz) were displayed on a screen in real-time and recorded in a logger (CR3000, Campbell Scientific Ltd., Shepshed, Leicestershire, UK). The power supply was provided by a lithium-ion battery.

The CH_4 mixing ratios were recorded on a predefined, 30 km long route through the urban area of Münster (Figure 1) that leads through a large part of the urban city area within the highly trafficked ring road (York-Ring to Hohenzollernring) and characteristic city districts (inner city, residential areas, commercial areas, Lake Aasee, Dortmund–Ems Canal). A tile pattern of 42 quadrants with edge lengths of 615 m was laid over the urban area (total area: 15,885,450 m^2). The quadrants were arranged in such a way that station MS4.9 was located in the corners of four quadrants. This allowed for the adjacent quadrants to be additionally analyzed with CH_4 mixing ratios associated with wind direction at MS4.9. The route of the MM covered each quadrant with distances between 384 m (F04) and 1337 m (L08; median: 670 m).

In contrast to sewer lines, which are placed under roadways, gas lines are located under the sidewalks along the buildings [40]. To keep the MM close to this potential source of CH_4, the bicycle route was planned to be on the edges of the roadways or, if possible, on bike paths on the sidewalks. Bicycle tours were made only when the following three conditions were fulfilled: dry weather, rising or already elevated background CH_4 mixing ratio, and stable stratification conditions.

2.3. Data Preparation and Peak Analysis

During the quality assurance of the MS4.9 and MM data, the data points associated with a signal strength <15% or other faulty diagnostic values (all values including "mirror cleaner motor failure" and/or "no laser signal detected") were dismissed. This eliminated 14.3% of the readings at MS4.9. The MM data were further filtered to eliminate the data points that were collected during a cruising speed of 1 m s^{-1} or less, which reduced the influence of varying mixing ratios during standstill times at traffic lights on the median of the entire quadrant area. This eliminated about 9.0% of the MM readings.

The CH_4 background mixing ratio at MS21 (B_{MS21}) was taken as the running 20-min average (1200 data points, centered) of the CH_4 mixing ratio at MS21.

At MS4.9 (not at MS21), peaks in the CH_4 mixing ratio were recorded regularly within certain time periods (see Section 3.1.2). For this reason, CH_4 mixing ratios at MS4.9 were analyzed by an adjusted peak analysis routine after Peitzmeier et al. [41]. The background mixing ratio $B_{MS4.9}$ (20-min average; 1200 data points, centered) originated from this analysis.

In a period on 17 December 2020, from 16:57 to 18:06 h (CET), the CH_4 mixing ratio at MS4.9 recorded an increase that was not recorded at MS21. This increase can thus be assumed to be a locally occurring peak. The routine used to determine $B_{MS4.9}$ followed this increase and, therefore, cannot mark the complete area of the increase as a peak area. For this reason, the computational $B_{MS4.9}$ value was adjusted to a constant 2.06 ppm over the

period mentioned. This adjustment defined a peak region with a duration of 48 min, which will henceforth be referred to as the "unique peak".

2.4. Estimation of the Source Strength

The source strength of the study area is estimated for the periods of MM trips. For this purpose, the following conditions and assumptions were formulated:

- Condition 1: Data show stable to extremely stable stratification conditions of the boundary layer during the MM trip.
- Condition 2: The CH_4 mixing ratios at MS21 and MS4.9 increase synchronously over the entire study area during the MM trip (detectable within the MM dataset).
- Assumption 1: The height of the stable boundary layer in Münster during the period under consideration is the same as at the DWD radiosonde in Essen at the time of the nearest ascent.
- Assumption 2: The increase in the CH_4 mixing ratio occurs equally throughout the height of the stable boundary layer.
- Assumption 3: The CH_4 source is located within the study area.

The area-averaged source strength of CH_4 was thus computed from the averaged increase (ppm h^{-1}) within the period of the lowest and highest mixing ratio of B_{MS21} and $B_{MS4.9}$ during the MM trips. The source strength of CH_4 was estimated for seven MM trips (applicable conditions 1 and 2) applying the general gas equation,

$$p \times V = n \times R \times T \quad (1)$$

and the following procedure: The air volume V in which all the CH_4 accumulates is defined as the study area (42 tiles) multiplied by the height of the stable boundary layer. With the data of temperature T, air pressure p (each averaged for the period of the lowest and highest mixing ratio of B_{MS21} and $B_{MS4.9}$), and the universal gas constant, the increasing number of moles n was determined. Under consideration of the molar mass of CH_4 (16.04 g mol^{-1}), the source strength of the study area (g h^{-1}) was calculated for each of the seven appropriate trips.

For locations exhibiting repeated elevated mixing ratios (EMR), the emission rate from the respective local sources was estimated using the method and equation described by Weller et al. [21]:

$$\ln(M\ CH_4) = -0.988 + 0.817 \times \ln(\text{emission rate } CH_4) \quad (2)$$

The emission rate was calculated for each trip and location using the highest measured differential mixing ratio (DMR) at the location minus the threshold for EMR detection (0.4 ppm) for M CH_4 (for descriptions of DMR and EMR, see Section 3.2). The representative emission rate of each location was defined as the mean value of all the single emission rates at that location. The mean emission rates of ground point sources were classified into small (<6 L min^{-1}), medium (6–40 L min^{-1}), and large (>40 L min^{-1}) sources, following the suggestions of von Fischer et al. [22].

The road network of the city of Münster has a total length of 1285 km. It can be classified into roads that are important for traffic (210 km), roads in the inner city area (25 km), roads in the remaining built-up area (760 km), and traffic areas in the undeveloped area, including service roads (290 km) [42]. The total emission rate of ground point sources (mostly from leaks in the gas pipelines) for the city of Münster (area: 303 km^2 [28]) was estimated by scaling the average emission rate of repeatedly measured EMR recorded over 30 km to the total length of the road network. This estimate was based on the assumption that the point sources are homogeneously distributed over the road network within built-up areas, including roads with significant traffic (total length of 995 km).

2.5. Statistical Evaluation and Software

Testing for the linear correlation of two variables was performed by determining the effect size (correlation coefficient; r) according to Pearson [43]. The classification into weak (r > 0.1), medium (r > 0.3), and strong (r > 0.5) correlations was conducted according to Cohen [44]. If one variable was present in larger time intervals, the other was adjusted by taking the mean value for the corresponding time interval.

Significant differences in medians in hourly observations of data in the diurnal cycle were derived from the 95% confidence interval around the median based on the interquartile range. Non-overlapping notches around two medians to be compared in boxplots provide strong evidence of a significant difference between the medians [45].

The average source strength of the study area is computed as the average of the source strengths for the seven periods of MM trips. The uncertainty of this average was estimated by bootstrapping seven samples out of the seven results and recalculating the average. The bootstrapping procedure was repeated 1000 times, and the standard deviation of the bootstrapped averages was computed.

All of the data analyses were performed using the software R [46]. Cartographic representation was performed using ArcMap [47]. All times are given as Central European Time (CET), which is UTC + 1 h.

3. Results and Discussion

3.1. Stationary Measurements

3.1.1. Background Mixing Ratios of CH_4 at the Stations MS21 and MS4.9

The two mixing ratio time series B_{MS21} and $B_{MS4.9}$ showed a strong linear correlation, with an effect strength of 0.88, and well-pronounced diurnal cycles (Figure 2): Relatively low background mixing ratios were detected in the morning hours, sometimes approaching the free tropospheric background mixing ratio (1.877 ppm [3]). Under these conditions, the atmospheric trace gas mixing ratios within the boundary layer are controlled to a large extent by the intensity of vertical mixing [48] and, thus, by mixing ratios of free tropospheric air rather than by CH_4 from near-ground emission sources that are well diluted in the boundary layer by thermal convection. Thus, over the morning and midday hours, both mixing ratios showed decreasing trends. The minima of the medians were reached within the 15th hour of the day for B_{MS21} and within the 18th hour for $B_{MS4.9}$. Later in the day, as the sun sets, the vertical temperature profile changes, and vertical mixing is reduced due to increasing stability (decreasing turbulence). This leads to an accumulation of trace gases that are emitted near the ground and to increasing CH_4 mixing ratios within the boundary layer [49]. Thus, the mixing ratios increased in the evening hours and during the nights until they reached a median peak within the eighth and ninth (B_{MS21}) or eighth ($B_{MS4.9}$) hour of the day. A common feature of the two datasets was that they had larger variances during the early morning than in the midday hours; the variances were smallest during the early evenings.

When comparing the two datasets on an hour-to-hour basis, $B_{MS4.9}$ showed larger mixing ratios than B_{MS21} throughout. $B_{MS4.9}$ reached values between 1.90 and 3.05 ppm with a median of 2.08 ppm. B_{MS21} ranged from 1.86 to 2.94 ppm with a median of 1.99 ppm. Thus, the difference between B_{MS21}–$B_{MS4.9}$ was, on average, −0.08 ppm, with a minimum of −0.71 ppm. Only 5% of the B_{MS21} mixing ratios exceeded those of $B_{MS4.9}$; the maximum difference between the stations was +0.35 ppm. Regarding ground-level emissions, an overall decrease in the CH_4 mixing ratio with increasing altitude is an indication that the ground-level CH_4 is regularly emitted within the study area [50]. This reasoning was further supported by comparing the mixing ratios of MM and B_{MS21}: 94% of the MM values were higher than the B_{MS21} values (see also Section 3.2).

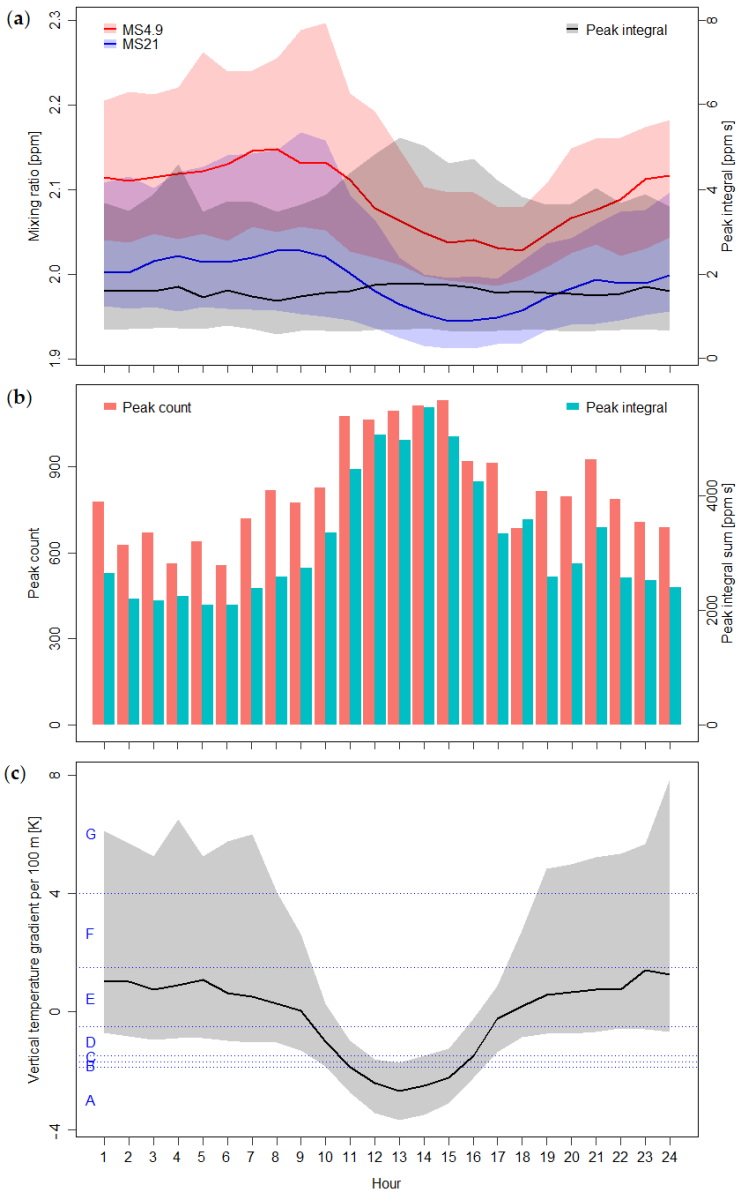

Figure 2. (**a**) Diurnal cycle of background mixing ratios at MS21 (B_{MS21}) and MS4.9 ($B_{MS4.9}$), and peak integral at MS4.9; lines represent median; shadows represent range between 25% quantile and 75% quantile; (**b**) Diurnal cycle of peak count and peak integral sum at MS4.9; (**c**) Diurnal cycle of the vertical temperature gradient; lines represent median, shadows represent range between 25% quantile and 75% quantile; blue: classification after Pasquill [38].

3.1.2. Peaks at Station MS4.9

The CH_4 mixing ratio at MS4.9 exhibited peaks 7.3% of the time. The peak durations were between 1 s and 14 min (median: 15 s). The unique peak (see Section 2.3 above) lasted 48 min. The median peak height was 0.21 ppm, and the maximum peak height was 5.17 ppm above $B_{MS4.9}$. The peak integral values ranged from just above the threshold (0.1 ppm s) to a maximum of 1210 ppm s during the unique peak. The second largest peak integral size was 110 ppm s; the median was 1.6 ppm s. The peak integral reached a median maximum at midday within the 13th hour of the day (Figure 2). The minimum of the median was reached within the eighth hour of the day. A diurnal cycle with a tendency toward a slight increase in the peak integral values around noon was apparent and was particularly evident in the upper quartile (Figure 2). The median of the eighth hour of the day differed significantly from the medians between the 12th and 15th hours of the day.

The peak count reached its maximum of 1130 peaks per hour in the 15th hour of the day (Figure 2), and the minimum peak counts were recorded during the early morning hours (the lowest count of 560 peaks within the sixth hour of the day). The diurnal cycle was even more pronounced for the sum of peak integrals, with a maximum of 5500 ppm s within the 14th hour of the day and a minimum of 2100 ppm s during the sixth hour (Figure 2).

3.1.3. Stratification Stability

Stable to extremely stable stratification conditions mainly occurred at night between the early evening and late morning (Figure 2). Between the 17th and 9th hours of the day, medians of the temperature gradient were in the stable stability range (class E). Over the midday hours, stable stratification conditions became rare, and unstable conditions predominated along with neutral ones. The medians between the 11th and 15th hours were in the unstable to very unstable stability range (class B and A, respectively).

Stable to extremely stable stratification conditions accounted for the largest share of the stability conditions in the entire period (49%, Table 1). At MS4.9, 41% of peaks had stable (class E, F, and G), 28% had neutral (class C and D), and 21% had unstable stratification conditions (class A and B).

Table 1. Stability conditions.

Stability Range	Class after Klug [36]/ Manier [37]	Class after Pasquill [38]	Temperature Gradient dT/dz [K/100 m]	Total Share [%]	Share during Peaks at MS4.9 [%]
Extremely stable		G	$4.0 \leq dT/dz$	17.8	7.1
Very stable	I	F	$1.5 \leq dT/dz < 4.0$	10.0	7.3
Stable	II	E	$-0.5 \leq dT/dz < 1.5$	21.0	26.6
Neutral	III/1	D	$-1.5 \leq dT/dz < -0.5$	18.5	23.2
Neutral	III/2	C	$-1.7 \leq dT/dz < -1.5$	3.5	4.9
Unstable	IV	B	$-1.9 \leq dT/dz < -1.7$	3.8	4.6
Very unstable	V	A	$dT/dz < -1.9$	17.3	16.4
NA				8.1	9.9

NA: missing data.

Thus, the stratification conditions during the peak events were only marginally different from the stratification conditions during the entire measurement period. As such, the occurrence of peak events at MS4.9 was not coupled to a specific form of stratification conditions. Therefore, several positions of the sources can be assumed on the windward side: Sources close to the ground and near the measuring station may lead to peaks at the measuring site even under conditions of low or very little turbulence, and sources further away and possibly elevated (e.g., a chimney) may also lead to peaks at the MS4.9 site, especially during conditions of pronounced turbulence.

3.1.4. Wind Direction

In Münster, the main wind direction (undisturbed wind field at MS21) was S–SW to W–SW 39% of the time. Northerly winds hardly occurred. Regarding the wind directions during high B_{MS21}, no specific pattern could be detected, as high B_{MS21} was associated with each wind direction at MS21. The winds originating from the inner-city area (directions E–S) made up 20% of wind directions in the class of the highest B_{MS21} percentile (>87.5–100%), suggesting that the city is not the only source of methane but that CH_4 sources are also present in the surrounding area. On a global scale, wetlands are the largest natural source of CH_4, accounting for 40% to 50% of total CH_4 emissions [51]. Other sources are found in landfills and agriculture; about two-thirds of the area around Münster is used for agriculture [52]. Agricultural emissions of CH_4 stem from animal husbandry and the use of farm manure such as slurry or solid manure. In addition, emissions are increasingly coming from biogas production [53]. Thus, we cannot exclude an advective supply of CH_4-enriched air to the measuring stations in the urban area.

In contrast to MS21, the wind directions at MS4.9 were dominated by directions of SE (15%), E–SE (13%), and S–SE (11%), adding up to a total share of 39%. Those wind directions mainly occurred during undisturbed SW wind conditions. Apparently, channeling effects were present at that site, driving the southwesterly winds around the power plants' building complex. Most of the peaks at MS4.9 (94%) occurred when the undisturbed wind direction was S-SW to W, and during 53% of these cases, the local wind direction at MS4.9 was SE, E–SE, and S–SE. The unique peak occurred during undisturbed SW winds and when the wind direction at MS4.9 was SE.

A higher frequency of undisturbed southwesterly winds (at MS21) was detected around noon. This diurnal pattern of wind directions is very similar to the diurnal pattern found for the number of peaks as well as the total of peak integrals. Thus, the occurrence of undisturbed SW wind is a possible explanation for the diurnal pattern of peak events at MS4.9. Assuming that the power plant complex was the source of the peaks, the diurnal variation of power plant operation could also provide an explanation for the temporal occurrence of the peaks. However, information on operating times could not be obtained from the power plant operator. The operator was also unable to provide an explanation for the occurrence of the unique peak, which was also recorded during undisturbed SW wind conditions. Thus, the cause or source of the peaks recorded at MS4.9 cannot be conclusively clarified.

3.2. Mobile Measurements (Point Sources and Emission Rates)

Eight of the ten trips occurred during stable to extremely stable stratification conditions (except for trips 2 and 3; Table S1). The average travel time per trip was about 2.25 h.

For the analysis of the MM data, we used the respective difference between the CH_4 mixing ratio of MM and B_{MS21} (CH_4 mixing ratio of MM-B_{MS21}), hereinafter referred to as the differential mixing ratio DMR; this procedure eliminated the temporal variance of B_{MS21} during individual trips. To indicate local increases in the CH_4 mixing ratio, all of the data points of a trip that showed a DMR > 0.4 ppm were defined as having an elevated mixing ratio (EMR). The locations where an EMR occurred were labeled according to the respective quadrant and the sum of trips with EMR. If a coordinate of a single data point occurred as an EMR during several trips, the sum of the elevated mixing ratios (SEMR) was formed for this coordinate with the number of trips concerned. Locations within the same quadrant with an identical number of trips with occurrences of EMR were distinguished by an additional letter.

For 94% of the cases, the CH_4 mixing ratio at MM exceeded the background mixing ratio B_{MS21} (positive DMR). For each quadrant, the median of the DMR of all trips was calculated and assigned to one of six levels (levels I to VI) in order to visualize the parts (quadrants) of the study area in which the ground-level CH_4 mixing ratios were higher relative to each other. The median DMR range was between 0.09 and 0.14 ppm. Two adjacent quadrants in the northeast of the study area, K05 and K06, were at the highest level VI (Figure 3), whereas one quadrant in the east, L07, and four quadrants in the south center of the study area (H09, I08, I09, and I10) were at level V. The medians of 16 quadrants, representing 38% of all quadrants, were in the lowest level I. These quadrants were located in the southeast of the study area along the canal, in the city center, north of Lake Aasee, and in the northwest of the study area.

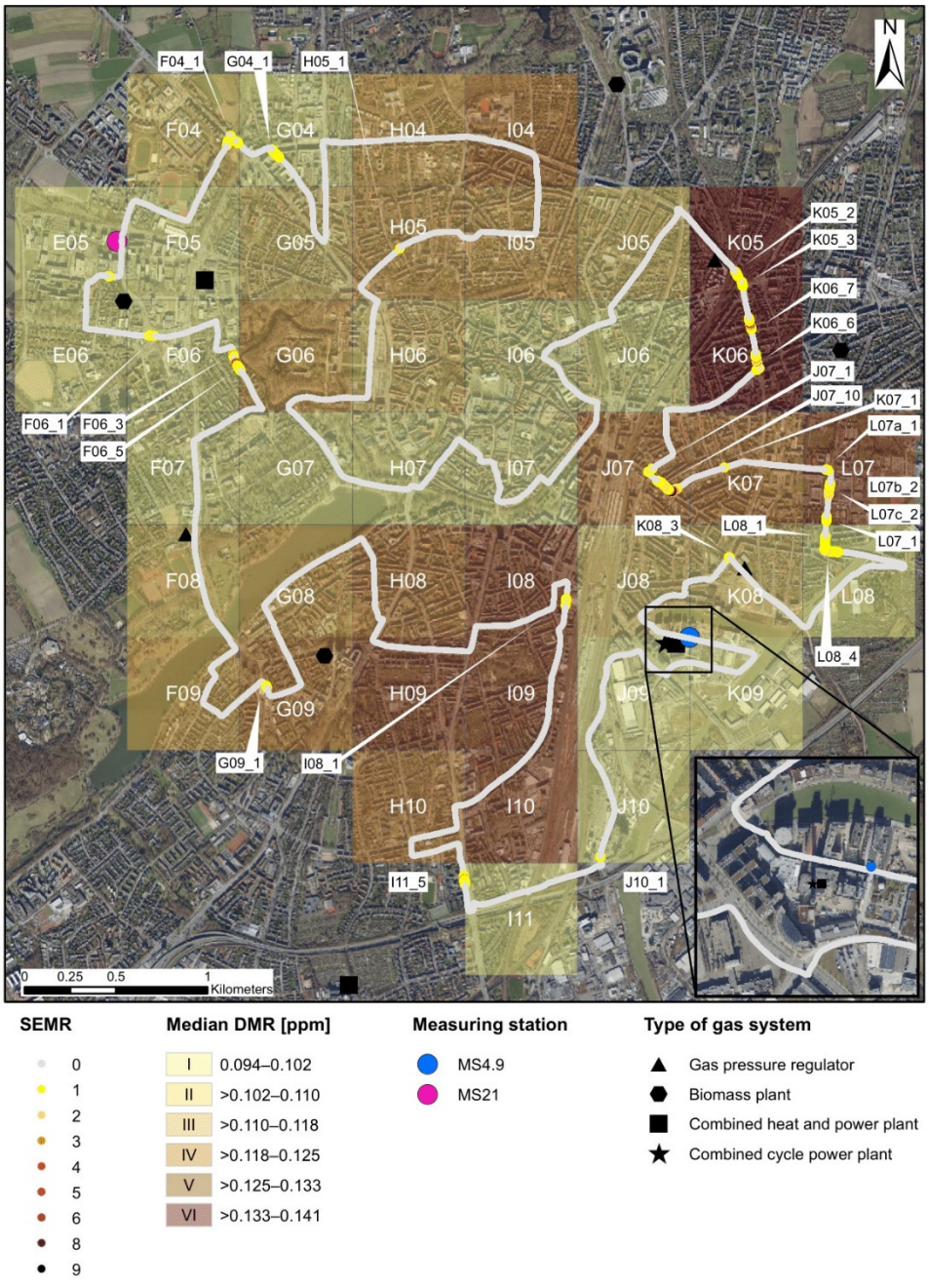

Figure 3. Overview of the route showing locations with occurrence of elevated mixing ratios (EMR) with indication of the sum of elevated mixing ratios (SEMR) and quadrant medians of the differential mixing ratio (DMR); Map source: DOP, © Geobasis NRW 2017, DL-DE->Zero-2.0, (http://www.govdata.de/dl-de/zero-2-0, accessed on 1 November 2021). URL: https://www.bezreg-koeln.nrw.de/brk_internet/geobasis/webdienste/geodatendienste/index.html (accessed on 1 November 2021); Locations of gas systems: MULNV NRW [54] and own sightings.

At 25 locations, the EMR were measured during at least one trip (Table S2). At 13 locations, EMR were repeatedly detected, corresponding to a rate of 0.43 km^{-1}. At 12 locations, the EMR occurred at the same coordinates (SEMR, see Section 3.2 above). Location J07_10 stands out, with EMR on every trip and maximum SEMR values of 9 within a subsection of 8 m (Figure 4). The maximum mixing ratio measured at J07_10 exceeded 47 ppm (Table S2).

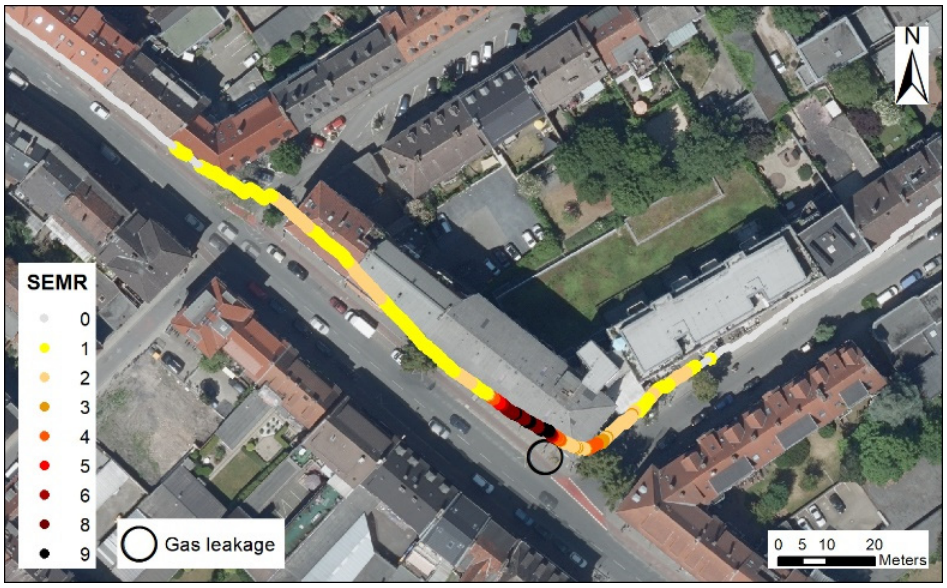

Figure 4. Location J07_10 with indication of SEMR along the route and localization of the leakage at the gas network; Note: depicted route deviates by a few meters to the north from the actually driven route; Map source: DOP, © Geobasis NRW 2017, DL-DE->Zero-2.0, (http://www.govdata.de/dl-de/zero-2-0, accessed on 1 November 2021). URL: https://www.bezreg-koeln.nrw.de/brk_internet/geobasis/webdienste/geodatendienste/index.html (accessed on 1 November 2021).

All locations at which EMR were repeatedly detected and, additionally, two locations with a single occurrence of high EMR (E05_1 and I08_1) were reported to the operator of the underground gas pipeline network (Stadtnetze Münster GmbH). At four locations, a total of five leaks in the gas network (low-pressure lines) were subsequently detected and identified as sources for EMR. At location J07_10, the leakage was repaired on 25 February 2021 [55]. Nevertheless, during the following four trips (trips 7 to 10), the MM still recorded EMR with a maximum DMR of 3.7 ppm. These remaining and repeatedly measured EMR, where no leakage was found, may have been caused by other, undetected leaks in the gas supply network or emissions from the sewer or leaks in the decentralized heating systems. Based on the isotopic compositions, Defratyka et al. [20] estimated the proportions of such point sources in Paris (France) to be 63% gas networks, 33% sewage systems, and 4% heating systems. Another potential cause for a single high EMR value may be passing natural gas-powered vehicles.

Quadrants K05 and K06 of the highest median level VI were conspicuous for sites with repeatedly detectable EMR. At locations K06_6 and K06_7, the point source could be confirmed as leakage in the gas network. Emissions from the gas grid were, thus, very likely responsible for the high median of quadrant K06 and possibly also for the median of quadrant K05. Another possible source of CH_4 was the localized gas pressure regulator in quadrant K05. In such installations, natural gas is transferred from the high-pressure network to the low-pressure network. In rare cases, controlled gas leakage occurs through a safety valve [55]. However, since no EMR were determined for the immediate vicinity of the gas pressure regulator, this plant is unlikely to be the (sole) reason for the (comparatively) high median of quadrant K05.

It was also noticeable that the four quadrants in the vicinity of the power plant complex at the harbor were classified in the lower levels I (J08, K08) and II (J09, K09). The power plant complex in quadrant J09 uses natural gas and biomethane. However, the EMR could not be determined in the vicinity of the power plant complex for any of the ten MM trips. This contrasts with the measurements at MS4.9, where sudden increases in the CH_4 mixing ratio (peaks) were detected 7.3% of the time during the measurement period, and the power plant complex was identified as the most likely source (see Section 3.1.4).

Relative to the distance traveled, the 15 identified point sources (at 13 locations) corresponded to a frequency of 0.5 km^{-1}. The emission rates were estimated to be 660 g h^{-1} on average (36 to 5500 g h^{-1}). Thus, the average emission rate of point sources per km of distance traveled was 22 g h^{-1} km^{-1}.

Weller et al. [21] developed their model for mobile measurements made from a car; their model assumes rather large distances between the source and the measuring device (average distance: 15.75 m). Because the MM predominantly drove on bicycle paths (often on the sidewalk), the distance between the MM and a gas leak or other point source was significantly shorter than the distance used by Weller et al. [21]. This could have led to a slight overestimation of the emission rate for each location and trip in the present study. To compensate for this potential overestimation, the mean value of all of the calculated emission rates per location was determined and then classified according to the method described by von Fischer et al. [22]: Accordingly, eight small (<240 g h^{-1}), five medium (240–1600 g h^{-1}), and one large source (>1600 g h^{-1}) were detected (Note that location J07_10 appeared as a large source before the leak was repaired and as a medium source afterward; Table S2).

In comparison to the results from four cities in the U.S. [21], the number of point sources per km traveled is highest in Münster (present work) at 0.5 km^{-1} (Table 2). However, due to the significantly longer distances traveled in those four U.S. cities, it is reasonable to assume that in those studies, the traveled areas included areas in which there was no gas network, making the number of point sources per km lower. In the emission rate per km traveled, however, the values in the comparison cities are higher than the value of 22 g h^{-1} km^{-1} determined in the present work. In Birmingham, it is almost twice as high, at 40 g h^{-1} km^{-1}, although the proportion of medium and large emission rates in Münster is significantly higher.

Table 2. Comparison of mobile-collected emission rates (Münster) with mobile-collected data from four cities in the U.S. [21].

	Münster	Birmingham	Anonymous City	Dallas	Pittsburgh
Route length [km]	30	589	916	1408	2466
Number of point sources *	15	168	275	414	460
Point sources per km traveled [km^{-1}]	0.50	0.29	0.30	0.29	0.19
Share of small emission rates [%] **	57	95	91	94	92
Share of medium emission rates [%] **	36	4	9	5	7
Share of large emission rates [%] **	7	1	0	1	1
Emission rate per km traveled [g h^{-1} km^{-1}]	22.0	40.4	33.6	34.8	23.2

* recorded on at least two different days; ** according to the proposed categorization by von Fischer et al. [22].

3.3. Methane Source Strength

The average increase in B_{MS21} and $B_{MS4.9}$ in the relevant periods of the seven appropriate MM trips was between 0.008 and 0.059 ppm h^{-1} (Table S3), resulting in an average source strength for the study area of 44,600 g h^{-1} (3700 to 85,000 g h^{-1}). Over the year, this would correspond to a source strength of 2.0 to 47 g m^{-2} a^{-1}, with an average of 24.6 g m^{-2} a^{-1}. The bootstrapped standard deviation is 2.8 g m^{-2} a^{-1} or 11%. Further uncertainties of the source strength estimate may originate from the experimental and computational procedure itself. For example, three assumptions had to be made in this study due to the lack of additional measured data (assumptions 1–3, see Section 2.4). More accurate and reliable estimates can only be made with more measurements, including the actual height of the stable boundary layer within the study area and covering all seasons of the year. Technical issues, such as the calibration of instruments, play a minor role in our uncertainty estimates. Overall, given the bootstrapped standard deviation of 11% and further uncertainties that we did not quantify, we estimate the overall uncertainty of the emission estimate to be ±20% (standard deviation).

Using a similar approach, Zimnoch et al. [49] estimated the annual CH_4 emissions in the urban area of Krakow, Poland, to be 13.6 g m^{-2} a^{-1}, which is about half the source strength estimated in the present work. Under stable stratification conditions, a clear vertical mixing ratio gradient of CH_4 within the boundary layer is usually observed (and was also observed in the present study). Therefore, for mixing ratio measurements near the surface, Zimnoch et al. [49] introduced a correction factor in their estimate of the source strength, whereby the correction factor was derived from the results of an analytical dispersion model by Sharan and Gopalakrishnan [56]. The correction factor infers the mixing ratio increase in the entire boundary layer from the measured mixing ratio increase near the ground by dividing the mean hourly mixing ratio increase near the ground by the mean CH_4 mixing ratio in the first 500 m of the atmosphere; the value of the correction factor is further guided by the aerodynamic roughness of the city under stable stratification conditions. Such a correction factor somewhat reduces the estimated source strength and, thus, provides a possible partial explanation for the difference in the source strength estimated by Zimnoch et al. [49] and that estimated in the present work.

Direct measurement of CH_4 fluxes can be made with eddy covariance measurements: A two-year campaign in the urban area of Łódź, Poland, showed CH_4 emissions of 18 g m^{-2} a^{-1} [57]. Significantly higher values were measured by Gioli et al. [9] in Florence, Italy, where CH_4 fluxes from urban areas were 69 g m^{-2} a^{-1}. In London, England, Helfter et al. [11] measured CH_4 emissions from urban areas of 72 g m^{-2} a^{-1}, with moderate seasonality observed during the three-year campaign. However, Helfter et al. [11] could not provide an explanation for the 21% increase in emissions during winter. It would be reasonable to assume that as winter temperatures fall, gas use increases due to increased heating activity, and with it, emissions increase. This could imply that the source strength (which in the present work was derived from the mixing ratio) increases in winter, thus resulting in an overestimate of the entire-year emission.

Upon scaling the average emission rate of repeatedly measurable point sources per km of distance traveled (22 g h^{-1} km^{-1}) to the total length of the road network within built-up areas (995 km, see Section 2.4), we estimated the total emission rate of point sources detected on the ground to be 21.9 kg h^{-1}. In terms of area, this corresponds to an annual emission rate of 0.64 g m^{-2} a^{-1}, which is 2.6% of the estimated source strength for the study area. This small fraction suggests that there are other CH_4 sources within the study area that either happened not to be detected on the ground, emit at higher altitudes, or are diffuse sources that do not lead to distinct, local peaks. The quadrant values do not indicate that the Dortmund–Ems Canal is a particular source of CH_4 within the study area. In contrast, gradual CH_4 emissions from Lake Aasee could be evident in the slightly elevated median values of the quadrants F08, F09, and G08.

According to the latest emissions data available (2017), the total CH_4 emissions of the city of Münster are estimated to be 80,000 t CO_2-equivalents. The energy sector, giving off 35% of CH_4 emissions, represents the second largest contributor to total CH_4 emissions in Münster (54% agriculture, 11% waste); in the energy sector, 93% of CH_4 emissions come from the gas industry, and 3.5% come from transport and households [30]. After converting the 2017 estimated value by a factor of 28 to account for the global warming potential of CH_4 [58], the total CH_4 emissions are 2,860 t a^{-1}, which corresponds to 9.4 g m^{-2} a^{-1} in relation to the area of Münster. In the current study, the average source strength of the study area was found to be much higher, at 24.6 g m^{-2} a^{-1}, exceeding the total CH_4 emissions reported in the emissions report by almost a factor of three. The emissions report estimates the annual CH_4 emissions from the gas industry to be 3.1 g m^{-2} a^{-1}; the determined emission rate from detectable point sources at ground level (0.64 g m^{-2} a^{-1}) corresponds to one-fifth of the annual CH_4 emissions from the gas industry.

4. Conclusions

In the present work, we obtained many insights into the dynamics of CH_4 in the urban boundary layer of Münster, Germany, by combining mobile and stationary measurement

techniques. For the first time (to our knowledge), an open path device such as the LI-7700 was used for mobile measurements. The present work has shown that the setup used here is well suited for measuring CH_4 mixing ratios on a mobile platform as well as for detecting leakages in the gas network and other unidentified point sources. By repeating the same trip multiple times during periods when the CH_4 background mixing ratio increased due to stable stratification conditions, a "heat map" of the study area (Figure 3) was created, highlighting the parts (quadrants) of the city that contribute comparatively more to the increase in background mixing ratio.

By estimating the source strength of the study area, considerably larger source strengths were found than previously reported in the city's emissions report. This suggests that there are undetected or unaccounted CH_4 sources inside the city of Münster. However, our estimates were made on the basis of various assumptions; therefore, further studies on the same topic should include local measurements of the stratification stability and height of the boundary layer. The "heat map" of the study area could be of valuable importance for finding a suitable and promising measurement site for an extended measurement campaign.

Coordinating and supplementing a measurement strategy with the infrastructure operator can improve or refine results. By using appropriate gas network plans, the mobile measurement setup used in the present work could prove to be useful when the gas network is undergoing review: The gas network is regularly checked by the operator according to worksheet DVGW G 465 [59] by checking the air directly above the ground surface for combustible gas using a handheld measuring device (carpet or bell probe). The check is carried out annually for high-pressure lines and every four years for low-pressure lines [55]. Because the MM can provide a large spatial coverage in a short time and because it has a high success rate in detecting point sources, the mobile measurement platform may become a suitable supplement to survey operations.

In principle, there is an urgent need for research to precisely quantify the direct CH_4 emissions or fluxes of a city. Measurements such as those presented here should be made in many cities and for longer time periods covering all seasons of the year. In addition, cities need access to targeted measurement setups that can directly record CH_4 fluxes by, for example, eddy covariance and assign their origins using isotope analysis. This will lead to more precise statements about the source strength and origin of urban CH_4; this information is critical for reducing urban CH_4 emissions into the atmosphere in a targeted manner and, thus, for protecting the climate.

Supplementary Materials: The following supporting information can be downloaded at: https://www.mdpi.com/article/10.3390/atmos13101596/s1, Table S1: Conditions during mobile measurements; Table S2: Locations with occurrence of elevated mixing ratios (EMR), measured maximum mixing ratio (MR) and estimated mean emission rate according to Weller et al. [21]. Table S3: Estimation of the source strength in the period of seven trips; time of start and time of end limit the period of stable stratification conditions.

Author Contributions: Conceptualization, methodology, validation, visualization: F.K.K., C.S., O.K.; software, formal analysis, investigation: F.K.K.; resources, supervision: C.S., O.K.; data curation: F.K.K., C.S.; writing—original draft preparation: F.K.K.; writing—review and editing: F.K.K., C.S., O.K.; All authors have read and agreed to the published version of the manuscript.

Funding: This research received no funding.

Institutional Review Board Statement: Not applicable.

Data Availability Statement: Data of stationary and mobile measurements are available from the authors on reasonable request. Further, publicly available datasets were utilized in this study. These data can be found at https://www.bezreg-koeln.nrw.de/brk_internet/geobasis/topographische_karten/aktuell/25000/index.html, https://www.bezreg-koeln.nrw.de/brk_internet/geobasis/webdienste/geodatendienste/index.html (Figures 1, 3 and 4, all accessed on 1 November 2021), and http://weather.uwyo.edu/upperair/sounding.html (radiosonde data, accessed on 23 August 2021).

Acknowledgments: We thank the Hafenkäserei Münster for granting us access to their premises to set up station MS4.9, and Celeste Brennecka for language editing of the manuscript.

Conflicts of Interest: The authors declare no conflict of interest.

References

1. Arias, P.A.; Bellouin, N.; Coppola, E.; Jones, R.G.; Krinner, G.; Marotzke, J.; Naik, V.; Palmer, M.D.; Plattner, G.-K.; Rogelj, J.; et al. Technical Summary. In *Climate Change 2021: The Physical Science Basis. Contribution of Working Group I to the Sixth Assessment Report of the Intergovernmental Panel on Climate Change*; Masson-Delmotte, V., Zhai, P., Pirani, A., Connors, S.L., Péan, C., Berger, S., Caud, N., Chen, Y., Goldfarb, L., Gomis, M.I., et al., Eds.; Cambridge University Press: Cambridge, UK; New York, NY, USA, 2021; pp. 33–144. [CrossRef]
2. Saunois, M.; Stavert, A.R.; Poulter, B.; Bousquet, P.; Canadell, J.G.; Jackson, R.B.; Raymond, P.A.; Dlugokencky, E.J.; Houweling, S.; Patra, P.K.; et al. The Global Methane Budget 2000–2017. *Earth Syst. Sci. Data* **2020**, *12*, 1561–1623. [CrossRef]
3. Tarasova, O.; Vermeulen, A. Greenhouse Gas Concentrations in the Atmosphere (Global Atmosphere Watch, GAW). In *United in Science 2020. A Multi-Organization High-Level Compilation of the Latest Climate Science Information*; Luterbacher, J., Paterson, L., Solazzo, K., Castonguay, S., Eds.; World Meteorological Organization (WMO): Geneva, Switzerland, 2020; p. 4.
4. Prather, M.J.; Holmes, C.D.; Hsu, J. Reactive greenhouse gas scenarios: Systematic exploration of uncertainties and the role of atmospheric chemistry. *Geophys. Res. Lett.* **2012**, *39*, 1–5. [CrossRef]
5. Shindell, D.; Kuylenstierna, J.C.I.; Vignati, E.; van Dingenen, R.; Amann, M.; Klimont, Z.; Anenberg, S.C.; Muller, N.; Janssens-Maenhout, G.; Raes, F.; et al. Simultaneously mitigating near-term climate change and improving human health and food security. *Science* **2012**, *335*, 183–189. [CrossRef] [PubMed]
6. Nisbet, E.G.; Fisher, R.E.; Lowry, D.; France, J.L.; Allen, G.; Bakkaloglu, S.; Broderick, T.J.; Cain, M.; Coleman, M.; Fernandez, J.; et al. Methane Mitigation: Methods to Reduce Emissions, on the Path to the Paris Agreement. *Rev. Geophys.* **2020**, *58*, 1–51. [CrossRef]
7. Ocko, I.B.; Sun, T.; Shindell, D.; Oppenheimer, M.; Hristof, A.; Pacala, S.W.; Mauzerall, D.L.; Xu, Y.; Hamburg, S.P. Acting rapidly to deploy readlily available methane mitigation measures by sector can immediately slow global warming. *Environ. Res. Lett.* **2021**, *16*, 054042. [CrossRef]
8. Zazzeri, G.; Lowry, D.; Fisher, R.E.; France, J.L.; Lanoisellé, M.; Grimmond, C.S.B.; Nisbet, E.G. Evaluating methane inventories by isotopic analysis in the London region. *Sci. Rep.* **2017**, *7*, 4854. [CrossRef]
9. Gioli, B.; Toscano, P.; Lugato, E.; Matese, A.; Miglietta, F.; Zaldei, A.; Vaccari, F.P. Methane and carbon dioxide fluxes and source partitioning in urban areas: The case study of Florence, Italy. *Environ. Pollut.* **2012**, *164*, 125–131. [CrossRef]
10. Townsend-Small, A.; Tyler, S.C.; Pataki, D.E.; Xu, X.; Christensen, L.E. Isotopic measurements of atmospheric methane in Los Angeles, California, USA: Influence of "fugitive" fossil fuel emissions. *J. Geophys. Res.* **2012**, *117*, D07308. [CrossRef]
11. Helfter, C.; Tremper, A.H.; Halios, C.H.; Kotthaus, S.; Bjorkegren, A.; Grimmond, C.S.B.; Barlow, J.F.; Nemitz, E. Spatial and temporal variability of urban fluxes of methane, carbon monoxide and carbon dioxide above London, UK. *Atmos. Chem. Phys.* **2016**, *16*, 10543–10557. [CrossRef]
12. Alvarez, R.A.; Zavala-Araiza, D.; Lyon, D.R.; Allen, D.T.; Barkley, Z.R.; Brandt, A.R.; Davis, K.J.; Herndon, S.C.; Jacob, D.J.; Karion, A.; et al. Assessment of methane emissions from the U.S. oil and gas supply chain. *Science* **2018**, *361*, 186–188. [CrossRef]
13. Saunois, M.; Bousquet, P.; Poulter, B.; Peregon, A.; Ciais, P.; Canadell, J.G.; Dlugokencky, E.J.; Etiope, G.; Bastviken, D.; Houweling, S.; et al. The global methane budget 2000–2012. *Earth Syst. Sci. Data* **2016**, *8*, 697–751. [CrossRef]
14. Brandt, A.R.; Heath, G.A.; Kort, E.A.; O'Sullivan, F.; Pétron, G.; Jordaan, S.M.; Tans, P.; Wilcox, J.; Gopstein, A.M.; Arent, D.; et al. Energy and environment. Methane leaks from North American natural gas systems. *Science* **2014**, *343*, 733–735. [CrossRef] [PubMed]
15. Pétron, G.; Karion, A.; Sweeney, C.; Miller, B.R.; Montzka, S.A.; Frost, G.J.; Trainer, M.; Tans, P.; Andrews, A.; Kofler, J.; et al. A new look at methane and nonmethane hydrocarbon emissions from oil and natural gas operations in the Colorado Denver-Julesburg Basin. *J. Geophys. Res.* **2014**, *119*, 6836–6852. [CrossRef]
16. Karion, A.; Sweeney, C.; Pétron, G.; Frost, G.; Michael Hardesty, R.; Kofler, J.; Miller, B.R.; Newberger, T.; Wolter, S.; Banta, R.; et al. Methane emissions estimate from airborne measurements over a western United States natural gas field. *Geophys. Res. Lett.* **2013**, *40*, 4393–4397. [CrossRef]
17. Nisbet, E.; Weiss, R. Atmospheric science. Top-down versus bottom-up. *Science* **2010**, *328*, 1241–1243. [CrossRef]
18. Plant, G.; Kort, E.A.; Murray, L.T.; Maasakkers, J.D.; Aben, I. Evaluating urban methane emissions from space using TROPOMI methane and carbon monoxide observations. *Remote Sens. Environ.* **2022**, *268*, 112756. [CrossRef]
19. Maazallahi, H.; Fernandez, J.M.; Menoud, M.; Zavala-Araiza, D.; Weller, Z.D.; Schwietzke, S.; von Fischer, J.C.; van der Denier Gon, H.; Röckmann, T. Methane mapping, emission quantification, and attribution in two European cities: Utrecht (NL) and Hamburg (DE). *Atmos. Chem. Phys.* **2020**, *20*, 14717–14740. [CrossRef]
20. Defratyka, S.M.; Paris, J.-D.; Yver-Kwok, C.; Fernandez, J.M.; Korben, P.; Bousquet, P. Mapping urban methane sources in Paris, France. *Environ. Sci. Technol.* **2021**, *55*, 8583–8591. [CrossRef]
21. Weller, Z.D.; Yang, D.K.; von Fischer, J.C. An open source algorithm to detect natural gas leaks from mobile methane survey data. *PLoS ONE* **2019**, *14*, e0212287. [CrossRef]

22. von Fischer, J.C.; Cooley, D.; Chamberlain, S.; Gaylord, A.; Griebenow, C.J.; Hamburg, S.P.; Salo, J.; Schumacher, R.; Theobald, D.; Ham, J. Rapid, vehicle-based identification of location and magnitude of urban natural gas pipeline leaks. *Environ. Sci. Technol.* **2017**, *51*, 4091–4099. [CrossRef]
23. Lamb, B.K.; Cambaliza, M.O.L.; Davis, K.J.; Edburg, S.L.; Ferrara, T.W.; Floerchinger, C.; Heimburger, A.M.F.; Herndon, S.; Lauvaux, T.; Lavoie, T.; et al. Direct and indirect measurements and modeling of methane emissions in Indianapolis, Indiana. *Environ. Sci. Technol.* **2016**, *50*, 8910–8917. [CrossRef] [PubMed]
24. Bilanzierung des Energieeinsatzes und der CO2-Emissionen für die Jahre 1990–2019. Available online: https://www.stadt-muenster.de/fileadmin/user_upload/stadt-muenster/67_klima/pdf/Bericht-Klimabilanz_Stadt_Muenster_2019.pdf (accessed on 2 March 2021).
25. Erzeugungsanlagen—Die Gas-und Dampfturbinen-Anlage (GuD). Available online: https://www.stadtwerke-muenster.de/unternehmen/energie/unser-angebot-fuer-sie/erzeugungsanlagen/gud.html (accessed on 5 October 2021).
26. Erzeugungsanlagen-Blockheizkraftwerke. Available online: https://www.stadtwerke-muenster.de/unternehmen/energie/unser-angebot-fuer-sie/erzeugungsanlagen/bhkw.html (accessed on 31 August 2021).
27. Mühlstein, J. *Starthelfer mit Effizienzbonus. Ein Gasmotoren-Blockheizkraftwerk mit 3,9 MW Elektrischer Leistung Ermöglicht den Stadtwerken Münster, ihr 100-MW-GuD-Heizkraftwerk bei Netzausfall Wieder in Betrieb zu Nehmen*; Energie & Management Verlagsgesellschaft mbH: Herrsching, Germany, 2009.
28. Wagner, R.; Tenberg, B. Energetische Infrastruktur. In *Masterplan 100% Klimaschutz für die Stadt Münster*; Jung Stadtkonzepte Stadtplaner & Ingenieure Partnerschaftsgesellschaft: Cologne, Germany, 2017; p. 38.
29. Versorgungsnetz Gas. Netzbeschreibung. Available online: https://www.stadtnetze-muenster.de/versorgungsnetze/versorgungsnetz-gas/ (accessed on 3 November 2021).
30. Filz, K.; Landesamt für Natur, Umwelt und Verbraucherschutz Nordrhein-Westfalen (LANUV NRW), Recklinghausen, North Rhine-Westphalia, Germany; Kohler, F.K.; University of Münster, North Rhine-Westphalia, Germany. Personal communication, 2021.
31. Koch, P.; Deutscher Wetterdienst (DWD), Essen, North Rhine-Westphalia, Germany; Kohler, F.K.; University of Münster, North Rhine-Westphalia, Germany. Personal communication, 2021.
32. Wurzler, S.; Landesamt für Natur, Umwelt und Verbraucherschutz Nordrhein-Westfalen (LANUV NRW), Recklinghausen, North Rhine-Westphalia, Germany; Kohler, F.K.; University of Münster, North Rhine-Westphalia, Germany. Personal communication, 2021.
33. Meyer, H.; Deventer, M.J.; Zhao, Y.; Klemm, O. CO_2 emissions from cities: Direct flux measurements versus the indirect budget approach. *Meteorol. Zeitschrift* **2019**, *28*, 379–387. [CrossRef]
34. Schaller, C.; Hofer, B.; Klemm, O. Greenhouse Gas Exchange of a NW German Peatland, 18 Years after Rewetting. *J. Geophys. Res. Biogeosci.* **2022**, *127*, e2020JG005960. [CrossRef]
35. Detto, M.; Verfaillie, J.; Anderson, F.; Xu, L.; Baldocchi, D. Comparing laser-based open- and closed-path gas analyzers to measure methane fluxes using the eddy covariance method. *Agric. For. Meteorol.* **2011**, *151*, 1312–1324. [CrossRef]
36. Klug, W. Method for determining atmospheric dispersion conditions from synoptic observations. *Staub-Reinhalt. Luft* **1969**, *29*, 143–147.
37. Manier, G. Vergleich zwischen Ausbreitungsklassen und Temperaturgradienten. *Meteorol. Rundsch.* **1975**, *28*, 6–11.
38. Pasquill, F. *Atmospheric Diffusion: The Dispersion of Windborne Material from Industrial and Other Sources*, 2nd ed.; Ellis Horwood: Chichester, UK, 1974.
39. University of Wyoming. College of Engineering. *Department of Atmospheric Science.* Available online: http://weather.uwyo.edu/upperair/sounding.html (accessed on 25 August 2021).
40. Stein, D. *Grabenloser Leitungsbau*, 1st ed.; Ernst & Sohn: Berlin, Germany, 2003.
41. Peitzmeier, C.; Loschke, C.; Wiedenhaus, H.; Klemm, O. Real-world vehicle emissions as measured by in situ analysis of exhaust plumes. *Environ. Sci. Pollut. Res.* **2017**, *24*, 23279–23289. [CrossRef]
42. Straßen: Straßenbau und-erhaltung. Available online: https://www.stadt-muenster.de/tiefbauamt/strassen/strassenbau-und-erhaltung#c49405 (accessed on 28 October 2021).
43. Fahrmeir, L.; Heumann, C.; Künstler, R.; Pigeot, I.; Tutz, G. *Statistik: Der Weg zur Datenanalyse*, 8th ed.; Springer Spektrum: Berlin/Heidelberg, Germany, 2016.
44. Cohen, J. *Statistical Power Analysis for the Behavioral Sciences*, 2nd ed.; Routledge: Abingdon, UK, 1988. [CrossRef]
45. Chambers, J.M.; Cleveland, W.S.; Kleiner, B.; Tukey, P.A. Comparing data distributions. In *Graphical Methods for Data Analysis*, 1st ed.; Chapman and Hall/CRC: Boca Raton, FL, USA, 1983. [CrossRef]
46. The R Project for Statistical Computing. Available online: https://www.R-project.org/ (accessed on 18 October 2021).
47. Environmental Systems Research Institute (ESRI). *ArcGIS Desktop 10.6.1.*; Environmental Systems Research Institute (ESRI): Redlands, CA, USA, 2018.
48. Emeis, S. Examples for the determination of turbulent (sub-synoptic) fluxes with inverse methods. *Meteorol. Z.* **2008**, *17*, 3–11. [CrossRef]
49. Zimnoch, M.; Godlowska, J.; Necki, J.M.; Rozanski, K. Assessing surface fluxes of CO_2 and CH_4 in urban environment: A reconnaissance study in Krakow, Southern Poland. *Tellus B Chem. Phys. Meteorol.* **2010**, *62*, 573–580. [CrossRef]

50. Querino, C.A.S.; Smeets, C.J.P.P.; Vigano, I.; Holzinger, R.; Moura, V.; Gatti, L.V.; Martinewski, A.; Manzi, A.O.; de Araújo, A.C.; Röckmann, T. Methane flux, vertical gradient and mixing ratio measurements in a tropical forest. *Atmos. Chem. Phys.* **2011**, *11*, 7943–7953. [CrossRef]
51. Tian, H.; Lu, C.; Ciais, P.; Michalak, A.M.; Canadell, J.G.; Saikawa, E.; Huntzinger, D.N.; Gurney, K.R.; Sitch, S.; Zhang, B.; et al. The terrestrial biosphere as a net source of greenhouse gases to the atmosphere. *Nature* **2016**, *531*, 225–228. [CrossRef] [PubMed]
52. Lammers, M.; Becker, T. *Landwirtschaft im Münsterland. Daten—Fakten—Analysen*, 2nd ed.; Landwirtschaftskammer Nordrhein-Westfalen: Münster, Germany, 2014.
53. Baumgarten, C.; Bilharz, M.; Döring, U.; Eisold, A.; Friedrich, B.; Frische, T.; Gather, C.; Günther, D.; Große Wichtrup, W.; Hofmeier, K.; et al. Umwelt und Landwirtschaft. In *Daten zur Umwelt | Ausgabe 2018*; Umweltbundesamt: Dessau-Roßlau, Germany, 2018.
54. NRW Umweltdaten vor Ort. Available online: https://www.uvo.nrw.de/ (accessed on 3 November 2021).
55. Schulze Brock, K.; Stadtnetze Münster GmbH, Münster, North Rhine-Westphalia, Germany; Kohler, F.K.; University of Münster, North Rhine-Westphalia, Germany. Personal communication, 2020 and 2021.
56. Sharan, M.; Gopalakrishnan, S.G. Mathematical modeling of diffusion and transport of pollutants in the atmospheric boundary layer. *Pure Appl. Geophys.* **2003**, *160*, 357–394. [CrossRef]
57. Pawlak, W.; Fortuniak, K. Eddy covariance measurements of the net turbulent methane flux in the city centre—Results of 2-year campaign in Łódź, Poland. *Atmos. Chem. Phys.* **2016**, *16*, 8281–8294. [CrossRef]
58. Filz, K.; Hoppe, D.; Laufhütte, T. *Treibhausgas-Emissionsinventar Nordrhein-Westfalen 2019. LANUV-Fachbericht 117*; Landesamt für Natur, Umwelt und Verbraucherschutz Nordrhein-Westfalen (LANUV NRW): Recklinghausen, Germany, 2021.
59. Deutscher Verein des Gas-und Wasserfaches e. V. (DVGW). *Technische Regel—Arbeitsblatt DVGW G 465-1 (A). Überprüfung von Gasrohrnetzen mit einem Betriebsdruck bis 16 Bar*; DVGW: Bonn, Germany, 2019.